Molecular mechanism of the flotillin complex in membrane microdomain organization

Ming-Ao Lu [1], Yunwen Qian [2], Liangwen Ma [3, 4], Qiang Guo[2, 4, §] & Ning Gao[1, 4, 5, 6, §]

[1] State Key Laboratory of Membrane Biology, Peking-Tsinghua Joint Center for Life Sciences, School of Life Sciences, Peking University, 100871, Beijing, China

[2] State Key Laboratory of Protein and Plant Gene Research, Peking-Tsinghua Center for Life Sciences, Academy for Advanced Interdisciplinary Studies, School of Life Sciences, Peking University, 100871, Beijing, China.

[3] Changping Laboratory Graduate Program, Academy for Advanced Interdisciplinary Studies, Peking University, 100871, Beijing, China.

[4] Changping Laboratory, Beijing, China

[5] National Biomedical Imaging Center, Peking University, 100871, Beijing, China

[6] Lead contact

[§] Correspondence: guo.qiang@pku.edu.cn (Q.G.), gaon@pku.edu.cn (N.G.)

Abstract

Flotillin-1 and flotillin-2, initially identified as markers of lipid rafts, assemble together as hetero-oligomers and facilitate the organization of flotillin membrane microdomains, which play a crucial role in various cellular processes, such as endocytosis, protein sorting, and vesicle trafficking. However, the molecular mechanisms underlying flotillin oligomerization and flotillin microdomain organization remain incompletely understood.

Here we present the cryo-electron microscopy structure of the human flotillin complex, at an overall resolution of 3.57 Å. It demonstrates that flotillin-1 and-2 are alternately arranged to form a 44-mer ring structure. This dome-shaped complex is hollow and sealed, attaching to the cytoplasmic leaflet of the plasma membrane and encompassing a circular domain with a diameter of approximately 30 nm. These structural features demonstrate a direct role for the flotillin complex in segregating the membrane to organize an isolated microdomain and also suggests a potential regulatory role in sequestering its interacting proteins. The cryo-electron tomography study further demonstrates the structural plasticity of the flotillin complexes in situ,

indicative of dynamic conformational changes during their functional activities. In addition, aggregations of the flotillin complexes on the plasma membrane or intracellular vesicles, are frequently observed. Our data suggest that the flotillin complex constitutes the basic structural unit of membrane microdomains, and the further clustering of flotillin complexes might facilitate the formation of larger and more elaborate membrane microdomains.

These findings enhance our understanding of the architecture of the SPFH family proteins and their common role in membrane microdomain organization, and more importantly, provide models for explaining the diverse functions of flotillin proteins in different biological processes.

Introduction

Plasma membranes, due to lipid-lipid and protein-lipid interactions and clustering, segregate into functional membrane microdomains (FMMs), commonly referred to as "lipid rafts" [1]. These small (ranging from 10 to 200 nm) platforms are discrete, heterogeneous, highly dynamic, and enriched with cholesterol and sphingolipids, and they compartmentalize critical cellular processes associated with the plasma membrane [2]. Flotillins, known markers of lipid rafts, exhibit a robust association with FMMs and play significant roles in FMM function [3]. There are two flotillin homologs in mammalian cells, FLOT1 and FLOT2. They are involved in diverse physiological functions, including endocytosis [4-6], signaling [7,8], protein trafficking[8,9] and cytoskeleton remodeling [10,11,12] (reviewed in [13,14]) . Flotillin overexpression has also been implicated in cell invasion and metastasis during tumorigenesis[15,14].

While FLOT1 has independent roles, such as regulating gene expression [16], it typically assembles with FLOT2 to form hetero-oligomers. FLOT1 and FLOT2 can be efficiently co-immunoprecipitated by each other, and extensively colocalize, forming small puncta in the plasma membrane that correspond to FLOT1/FLOT2 FMMs [17]. The microdomains containing FLOT1/FLOT2 complexes are laterally mobile within the plasma membrane, and can be internalized into the cell with various cargos [5,17-20] or secreted out of the cell [21,22]. Fyn kinase [6] and RAB31 [21] respectively regulate the roles of flotillins in endocytosis and exosome secretion. The overexpression of flotillins disrupts membrane domain homeostasis, promoting plasma membrane invagination and endocytosis towards late endosomes, thus altering the trafficking of various cargos[17].

Flotillin belongs to the SPFH (Stomatin, Prohibitin, Flotillin, and HflK/C) protein family, which shares a conserved structural organization that comprises an SPFH domain and a subsequent long α-helix (coiled-coil, CC domain). These family members serve as markers of lipid raft-like microdomains across various subcellular compartments, such as prohibitins (PHBs) in the inner mitochondrial membrane and erlins in the endoplasmic reticulum (ER) [23]. Recent findings suggest

that SPFH domain-containing proteins can self-oligomerize and anchor to membranes [23-26]. Flotillins lack transmembrane domains yet exhibit robust association with membranes. This association is facilitated by a combination of post translation modifications: S-palmitoylation of a few cysteine residues in their N-terminal domains and an N-terminal myristoylation specific for FLOT2[10]. In addition, a putative cholesterol recognition/interaction amino acid (CRAC) motif within their SPFH domain may also facilitate membrane association [27]. The long α-helices presented in both FLOT1 and FLOT2 contribute to their oligomerization [28]. However, the structural basis for FLOT1 and FLOT2 oligomerization and the molecular mechanisms underlying the formation of FLOT1/FLOT2 microdomains remain unknown.

In this study, by employing cryo-electron microscopy, we elucidate the high-resolution structure of the flotillin complex and in situ architecture of the flotillin microdomain. These findings provide novel insights into the crucial roles of flotillins in membrane microdomain organization and function, opening new avenues for the further exploration of their mechanisms in various cellular functions.

Results and discussion

FLOT1/FLOT2 complex preparation and structural determination

FLOT1 and FLOT2 were co-expressed in HEK293F cells, and a FLAG tag was placed at the C-terminus of FLOT1 for the complex purification from solubilized membrane fractions. To further increase sample homogeneity, glycerol density gradient centrifugation was performed and peak fractions were used for structural analysis (Fig. S1a). The distribution of FLOT1 and FLOT2 in the glycerol fractions was concentrated in high molecular-weight fractions, and each fraction was examined using negative-staining electron microscopy (nsEM) (Fig. S1b). The FLOT1/FLOT2 complex exhibited trapezoid-like shapes (side view) (Fig. S1c) and round shapes (top/bottom view) in the nsEM images. From the nsEM images, some complexes were seen to attach to membrane vesicles with the lower bottom of the trapezoids (Fig. S1d).

Subsequent cryo-electron microscopy (cryo-EM) analysis confirmed that FLOT1/FLOT2 particles resembled a dome-like structure. However, a significant portion of particles exhibited irregularly deformations, and some classes from early 3D classification even show ruptures in the structures (Fig. S2). One possible explanation is that flotillin domes are very large and their walls are relatively thin such that the structures could not remain as a rigid body. Due to the heterogeneity of the particles, the alignment of 2D particle images during single-particle cryo-EM 3D reconstruction was challenging and resulted in low-resolution density maps. To obtain a high-

resolution refinement, we eliminated deformed particles during data processing (see methods for details). Only those particles without apparent deformations (less than 2% of all particles) were included in the analysis. C22 symmetry was imposed during refinement (Fig. S2a), which resulted in a final density map of overall 3.57 Å resolution (Fig. S3). Atomic models were built de novo in this global map for most of the sequences of FLOT1 and FLOT2. The membrane associated regions (SPFH domains) were built using the AlphaFold2 [29] predicted structures as references (see methods for details).

The structure of the FLOT1/FLOT2 complex shows that it forms a dome-like structure on the membrane. The dome is composed of 22 copies of FLOT1-FLOT2 dimers arranged in a circular manner, giving rise to the C22 symmetry (Fig. 1). When viewed from the side, the FLOT1/FLOT2 structure can be divided into three parts: the base region (~70 Å high), the wall region (~140 Å high), and the roof region (~175 Å wide) (Fig. 1c). The base region comprises the SPFH domains of FLOT1 and FLOT2, which are associated to the membrane (density of detergent micelles shown in Fig. 1c). The wall region of the structure is formed by a single layer of parallel-arranged helices, creating a helical barrel. The dome structure is tightly sealed in both the base region and wall region, with the inner leaflet of the plasma membrane serving as the bottom. At the center of the roof region, there appears to be a hole about 40 Å wide (Fig. 1a). However, in maps imposed with C1 symmetry, densities appeared in the hole (Fig. S2a), likely corresponding to the unresolved C-terminus of FLOT2.

Structures of FLOT1 and FLOT2 and their membrane-associated domains

With approximately 48% sequence identity (Fig. S4–5), FLOT1 and FLOT2 have nearly identical 3D structures (Fig. 2a–f). The structures of both proteins can be divided into five domains, including two SPFH domains (SPFH1 and SPFH2), two coiled-coil domains (CC1 and CC2), and a C-terminal domain (CTD) (Fig. 2a, d), similar to the structure of HflK/C complex[26,30,31].

The SPFH1 domains, consisting of five antiparallel β-strands (β1–β5) (Fig. 2c, f), are peripheral membrane domains, half of which are buried in the detergent micelle (Fig. 2b, e, g–j). The SPFH1 domains contain many aromatic residues (Fig. 2j, S4a), such as F2, F3, F16 and F30 of FLOT1, and W32, W34, W36 and W37 of FLOT2. Therefore, the bottom rim of the FLOT1/FLOT2 complex is highly hydrophobic (Fig. S6a). Most importantly, cystine residues (C34 of FLOT1; C4, C19 and C20 of FLOT2), which were reported to be palmitoylated [10], are all buried in membrane (Fig. 2j). Furthermore, the glycine residue (G2) of FLOT2 is myristoylated, and its mutation (G2A) makes FLOT2 soluble rather than membrane-associated [10]. All these characteristics play important roles in membrane association. The 44 circularly arranged SPFH1 domains define a membrane area of

~700 nm^2 in the inner leaflet of the membrane, which is isolated from its surroundings (Fig. 2g, h). This highlights the physiological significance of the FLOT1/FLOT2 complex in membrane compartmentation. The structures of the SPFH2 domains in FLOT1 and FLOT2 are similar to those of other SPFH family members that have been previously reported [26,30,32-34], featuring an α/β-fold consisting of three β-strands and four α-helices.

Following the SPFH domains, the CC1 domains (α5) of FLOT1 and FLOT2 both contain 189 residues, which are significantly longer than those of other SPFH family members (Fig. S5), and they align perfectly to form a right-handed helical barrel and serve as the dome wall (Fig. 2k–m). Besides, there are two small bends at the sites of Pi-helical (π) and 3_{10}-helical (η) motifs of CC1 domains (Fig. 2b, e), constituting the two hoops observed in the side view of the dome (Fig. 1c).

After a nearly 90° bend at the end of CC1 domains, the CC2 domains and the CTDs of both flotillins make up the roof of the dome (Fig. 3a–e). With a common β-strand (β10) at the center of the roof region, the following sequences in CTDs of FLOT1 and FLOT2 have distinct structures, similar to the HflK/C complex [26,30]. Helices (α7) in CTDs of FLOT1 are reversed towards the end of CC1 domains, and the very C-terminus is exposed in the cytoplasmic space (Fig. 3b, c). Putative helices (α7) in CTDs of FLOT2 are not fully resolved in the map, but residual densities suggest that they should be buried inside the FLOT1/FLOT2 dome (Fig. 3b, c). This observation is consistent with the finding that the FLOT1/FLOT2 complex could not be purified through a FLAG tag at the C-terminus of FLOT2.

Oligomerization of FLOT1 and FLOT2

22 copies of FLOT1 and 22 copies of FLOT2 are alternately arranged to form a dome-like structure, denoted as F1(1)–F1(22) and F2(1)–F2(22), respectively. FLOT1 and FLOT2 form two unique heterodimeric interfaces corresponding to the two forms of FLOT1/FLOT2 dimers: F1-F2 and F2-F1.

In the SPFH1 domains (Fig. S6b–e), the residues of FLOT1 and FLOT2 involved in inter-subunit interactions are conserved (Fig. S4a), indicating that there is no specificity in the selection of FLOT1 or FLOT2 for oligomerization based on SPFH1 domains. The interfaces of adjacent SPFH2 domains are characterized by oppositely charged surface patches, which exhibit a clear charge complementarity (Fig. S6f–i). These charged patch pairs dictate that FLOT1 and FLOT2 must be alternately arranged to form a complete complex. The interactions between parallel CC1 domains are evenly distributed along the entire helices, with no preference for either polar (Fig. S7a–c) or hydrophobic interactions (Fig. S7d–f).

In the roof region, the 44 CC2 domains from FLOT1/FLOT2 point towards the center as α-helical "spokes", forming the bottom layer of the roof (Fig. 3c–e). The subsequent 44 short β-strands (β10) form a central β-barrel "hub" (Fig. 3a–c). Following this, 22 helices (α7) of FLOT1 fold back towards the rim, forming another set of α-helical "spokes" that make up the top layer of the roof (Fig. 3c, e). In contrast, the 22 C-termini of FLOT2 are buried inside the dome (Fig. 3b, c). The interactions involved in the formation of the roof region are mainly hydrophobic, both at the interface between two layers of α-helical "spokes" (Fig. 3e) and between adjacent CC2 domains (Fig. 3d). One "spoke" of the top layer (the helix (α7) of F1(2)) contacts four "spokes" of the bottom layer (CC2 domains of F1(1), F2(1), F1(2) and F2(2)) (Fig. 3c, e). It was previously shown that the C-terminal truncation could disrupt the formation of the HflK/C complex [30]. Similarly, progressive truncation of the C-terminal sequences did lead to impaired formation of the dome structures. Removal of the CC2 domains and their following sequences resulted in a significant increase of FLOT1/2 in lower molecular-weight fractions (Fig. S8).

In the FLOT1/FLOT2 complex, while the SPFH1 and SPFH2 domain are vertical relatively to the membrane plane, the CC1 domains packs against each other in a super-helical pattern (right-handed). The turning points between SPFH2 domains and CC1 domains, are determined by multiple hydrophilic interactions. Specifically, the negatively charged pocket formed by residues E63, E121 and Y163 of F2(1) accommodates the positively charged residue R168 of F1(1) (Fig. 3f). Similarly, H59, E118 and Y160 of F1(2) form a pocket for Q171 of F2(1) (Fig. 3g). Furthermore, these polar residues are highly conserved between the two flotillin homologs (Fig. S5). However, mutations of the four residues in these interfaces (Fig. S8) did not abolish the formation of the dome structure. Importantly, Y160 of FLOT1 and Y163 of FLOT2 were reported to be the substrates of Src family tyrosine kinase Fyn, and mutation of these residues to phenylalanine prevents Fyn-induced flotillins internalization [6,12]. An additional phosphate group on Y160 of FLOT1 or Y163 of FLOT2 in these pockets might be able to change the tilt angle between the SPFH domains and CC1 domains, implying a phosphorylation-based regulation on the overall structure of the FLOT1/2 complex.

In situ structure of FLOT1/FLOT2 complex

To facilitate in situ structural analysis, a Jurkat T cell line stably expressing FLOT1-EGFP and FLOT2-mCherry was generated. Flotillin complexes are known to exhibit a polarized distribution in T cells, localizing to caps, uropods, and the immune synapse during resting[35], migrating[11], and conjugated stages[8], respectively. Consistently, our fluorescent confocal imaging results show that FLOT1 and FLOT2 were co-localized in caps or uropods of Jurkat T cells (Fig. 4a, S9a). Additionally,

glycerol density gradient centrifugation assay confirmed that the fluorescent tags did not disrupt the assembly of FLOT1/FLOT2 complexes (Fig. S9b).

Guided by the fluorescent signals of FLOT1-EGFP and FLOT2-mCherry, lamellae were prepared at regions enriched in FLOT1/FLOT2 complexes (Fig. 4b). Subsequent tomographic reconstructions revealed a cellular periphery with a clearly visible plasma membrane, consistent with the known localization of FLOT1/FLOT2 complexes in caps or uropods (Fig. 4c, d). Notably, a significant number of hollow dome-shaped structures with heights of approximately 20 nm were observed attached to the cytosolic side of the plasma membrane (Fig. 4e, S11b), resembling our cryo-EM structure of the FLOT1/FLOT2 complex. To validate the identity of these structures, sub-tomogram averaging was performed. While the limited data size restricts the final map resolution and prevents definitive identification based solely on structure, the overall shape of the structure in conjunction with the correlative light and electron microscopy (CLEM) results strongly suggest their formation by the FLOT1/FLOT2 complex (Fig. 4f, g).

Individual structures within the tomograms revealed additional electron densities within the complexes (Fig. 4e). These densities likely correspond to various interacting partner proteins. However, they were absent in the averaged structure, suggesting a high heterogeneity of partner proteins with the domes. Additionally, a significant degree of structural variation was observed among the individual complexes (Fig. S10a–b). This observation aligns with the findings from purified samples (Fig. S2b–d, S10c–d), further supporting the notion that the flotillin complexes are highly dynamic in nature. This property might be essential for the FLOT1/FLOT2 complex's cellular functions.

Organization model of flotillin membrane microdomains

The tomographic data offered a unique opportunity to investigate the spatial distribution and membrane preferences of flotillin complexes in situ. A majority of the observed flotillin complexes existed as individual units. Given the substantial membrane area encompassed by the dome-shaped complex, it is conceivable that the complex, along with its associated proteins, contribute to the organization of a specialized membrane microdomain. Notably, we also observed clusters of flotillin complexes on extracellular vesicles (Fig. 5a), endosomes and plasma membrane (Fig. 5b), which aligns with the presence of larger membrane microdomains implicated in exosome formation[36] and endocytosis[5,6,17], respectively.

The flotillin complexes show no preference for membrane curvature (Fig. S11). Despite of the enrichment of flotillin complexes on highly curved vesicles in purified sample (Fig. S11a) and endosomes in situ (Fig. S11d), the in vitro averaged structures of non-vesicle-associated particles

exhibited a slightly concave membrane (Fig. S11e). Additionally, the in situ flotillin complexes were observed on both concave and convex membrane surfaces, both of which were relatively flat (Fig. S11b). We also happened to find a FLOT1/FLOT2 complex on a highly concave membrane surface inside a tiny vesicle (Fig. S11c), even though it might be inside an apoptosis cell and undergoing degradation in endolysosomes according to the cellular context in situ. Thus, the mechanisms that drive membrane curvature during flotillin mediated endocytosis require further investigation.

Here, we present a new model of flotillin membrane microdomain (Fig. 5c): The membrane encompassed by the complex is laterally segregated as a basic unit of the microdomain (30-nm in diameter). Together with specifically associated lipids and proteins, the flotillin membrane microdomain could exert diverse functions in different cellular processes. Under certain conditions, the flotillin complexes could cluster to form larger membrane microdomains (more than 200-nm in diameter), serving as a platform for endocytosis and inter-membrane trafficking.

Acknowledgements

We thank Dr. Chengying Ma and Dr. Ningning Li for invaluable advice in cryo-EM data processing, Wenjing Du, Dr. Changdong Qin, Xing Wang and Dr. Wenhong Jiang for aiding in cryo-ET experiments, and all members of the Gao Lab and Guo Lab for insightful discussions. We thank the Core Facilities at the School of Life Sciences, Peking University for help with negative staining EM and confocal microscopy; the Cryo-EM Platform and the Electron Microscopy Laboratory of Peking University for help with data collection; the High-performance Computing Platform of Peking University for help with computation; and the National Center for Protein Sciences at Peking University for assistance in key experiments. This work was supported by National Natural Science Foundation of China (Grant # 92354306), and by the Ministry of Science and Technology of China and Changping Laboratory.

Author contributions

N.G. and Q.G. designed and supervised the project; M.L. purified the sample with help from L.M.; M.L. carried out all other experiments. Y.Q. and M.L. conducted cryo-ET data analysis. M.L. and Q.G. prepared figures and wrote the manuscript. N.G. and Q.G. revised the manuscript. All the authors approved the manuscript.

Competing interests

The authors declare no competing interests.

Data and materials availability

The cryo-EM volume and the structure coordinates have been deposited in the Electron Microscopy Data Bank and the Protein Data Bank under accession codes EMD-XXXX and XXXX.

Supplementary Materials

Materials and Methods

Figs. S1 to S11

Tables S1

References

1 Simons, K. & Ikonen, E. Functional rafts in cell membranes. *Nature* **387**, 569-572 (1997). https://doi.org:10.1038/42408

2 Pike, L. J. Rafts defined: a report on the Keystone symposium on lipid rafts and cell function. *Journal of Lipid Research* **47**, 1597-1598 (2006). https://doi.org:https://doi.org/10.1194/jlr.E600002-JLR200

3 Bickel, P. E. *et al.* Flotillin and epidermal surface antigen define a new family of caveolae-associated integral membrane proteins. *J Biol Chem* **272**, 13793-13802 (1997). https://doi.org:10.1074/jbc.272.21.13793

4 Schneider, A. *et al.* Flotillin-dependent clustering of the amyloid precursor protein regulates its endocytosis and amyloidogenic processing in neurons. *J Neurosci* **28**, 2874-2882 (2008). https://doi.org:10.1523/JNEUROSCI.5345-07.2008

5 Glebov, O. O., Bright, N. A. & Nichols, B. J. Flotillin-1 defines a clathrin-independent endocytic pathway in mammalian cells. *Nat Cell Biol* **8**, 46-54 (2006). https://doi.org:10.1038/ncb1342

6 Riento, K., Frick, M., Schafer, I. & Nichols, B. J. Endocytosis of flotillin-1 and flotillin-2 is regulated by Fyn kinase. *J Cell Sci* **122**, 912-918 (2009). https://doi.org:10.1242/jcs.039024

7 Abousawan, J., Orofiamma, L. A., Fairn, G. D. & Antonescu, C. N. HER2 expression defines unique requirements for flotillin and c-Src in EGFR signaling. *J Cell Sci* **136** (2023). https://doi.org:10.1242/jcs.260133

8 Redpath, G. M. I. *et al.* Flotillins promote T cell receptor sorting through a fast Rab5-Rab11 endocytic recycling axis. *Nat Commun* **10**, 4392 (2019). https://doi.org:10.1038/s41467-019-12352-w

9 Meister, M. *et al.* Regulation of cargo transfer between ESCRT-0 and ESCRT-I complexes by flotillin-1 during endosomal sorting of ubiquitinated cargo. *Oncogenesis* **6**, e344 (2017). https://doi.org:10.1038/oncsis.2017.47

10 Neumann-Giesen, C. *et al.* Membrane and raft association of reggie-1/flotillin-2: role of myristoylation, palmitoylation and oligomerization and induction of filopodia by overexpression. *Biochem J* **378**, 509-518 (2004). https://doi.org:10.1042/BJ20031100

11 Affentranger, S., Martinelli, S., Hahn, J., Rossy, J. & Niggli, V. Dynamic reorganization of flotillins in chemokine-stimulated human T-lymphocytes. *BMC Cell Biol* **12**, 28 (2011). https://doi.org:10.1186/1471-2121-12-28

12 Neumann-Giesen, C., Fernow, I., Amaddii, M. & Tikkanen, R. Role of EGF-induced tyrosine phosphorylation of reggie-1/flotillin-2 in cell spreading and signaling to the actin cytoskeleton. *J Cell Sci* **120**, 395-406 (2007). https://doi.org:10.1242/jcs.03336

13 Kwiatkowska, K., Matveichuk, O. V., Fronk, J. & Ciesielska, A. Flotillins: At the Intersection of Protein S-Palmitoylation and Lipid-Mediated Signaling. *Int J Mol Sci* **21** (2020). https://doi.org:10.3390/ijms21072283

14 Gauthier-Rouviere, C., Bodin, S., Comunale, F. & Planchon, D. Flotillin membrane domains in cancer. *Cancer Metastasis Rev* **39**, 361-374 (2020). https://doi.org:10.1007/s10555-020-09873-y

15 Planchon, D. *et al.* MT1-MMP targeting to endolysosomes is mediated by upregulation of flotillins. *J Cell Sci* **131** (2018). https://doi.org:10.1242/jcs.218925
16 Jang, D., Kwon, H., Choi, M., Lee, J. & Pak, Y. Sumoylation of Flotillin-1 promotes EMT in metastatic prostate cancer by suppressing Snail degradation. *Oncogene* **38**, 3248-3260 (2019). https://doi.org:10.1038/s41388-018-0641-1
17 Frick, M. *et al.* Coassembly of flotillins induces formation of membrane microdomains, membrane curvature, and vesicle budding. *Curr Biol* **17**, 1151-1156 (2007). https://doi.org:10.1016/j.cub.2007.05.078
18 Stuermer, C. A. *et al.* Glycosylphosphatidyl inositol-anchored proteins and fyn kinase assemble in noncaveolar plasma membrane microdomains defined by reggie-1 and -2. *Mol Biol Cell* **12**, 3031-3045 (2001). https://doi.org:10.1091/mbc.12.10.3031
19 Saslowsky, D. E. *et al.* Intoxication of zebrafish and mammalian cells by cholera toxin depends on the flotillin/reggie proteins but not Derlin-1 or -2. *J Clin Invest* **120**, 4399-4409 (2010). https://doi.org:10.1172/JCI42958
20 Singh, J. *et al.* Cross-linking of the endolysosomal system reveals potential flotillin structures and cargo. *Nat Commun* **13**, 6212 (2022). https://doi.org:10.1038/s41467-022-33951-0
21 Wei, D. *et al.* RAB31 marks and controls an ESCRT-independent exosome pathway. *Cell Research* **31**, 157-177 (2021). https://doi.org:10.1038/s41422-020-00409-1
22 Strauss, K. *et al.* Exosome secretion ameliorates lysosomal storage of cholesterol in Niemann-Pick type C disease. *J Biol Chem* **285**, 26279-26288 (2010). https://doi.org:10.1074/jbc.M110.134775
23 Browman, D. T., Hoegg, M. B. & Robbins, S. M. The SPFH domain-containing proteins: more than lipid raft markers. *Trends Cell Biol* **17**, 394-402 (2007). https://doi.org:10.1016/j.tcb.2007.06.005
24 Ma, C. *et al.* Structural insights into the membrane microdomain organization by SPFH family proteins. *Cell Research* **32**, 176-189 (2022). https://doi.org:10.1038/s41422-021-00598-3
25 Langhorst, M. F., Reuter, A. & Stuermer, C. A. Scaffolding microdomains and beyond: the function of reggie/flotillin proteins. *Cell Mol Life Sci* **62**, 2228-2240 (2005). https://doi.org:10.1007/s00018-005-5166-4
26 Qiao, Z. *et al.* Cryo-EM structure of the entire FtsH-HflKC AAA protease complex. *Cell Rep* **39**, 110890 (2022). https://doi.org:10.1016/j.celrep.2022.110890
27 Sonnino, S. & Prinetti, A. Membrane domains and the "lipid raft" concept. *Curr Med Chem* **20**, 4-21 (2013).
28 Solis, G. P. *et al.* Reggie/flotillin proteins are organized into stable tetramers in membrane microdomains. *Biochem J* **403**, 313-322 (2007). https://doi.org:10.1042/BJ20061686
29 Tunyasuvunakool, K. *et al.* Highly accurate protein structure prediction for the human proteome. *Nature* **596**, 590-596 (2021). https://doi.org:10.1038/s41586-021-03828-1
30 Ma, C. *et al.* Structural insights into the membrane microdomain organization by SPFH family proteins. *Cell Res* **32**, 176-189 (2022). https://doi.org:10.1038/s41422-021-00598-3

31 Tanaka, H. *et al.* The structure of rat liver vault at 3.5 angstrom resolution. *Science* **323**, 384-388 (2009). https://doi.org:10.1126/science.1164975
32 Yokoyama, H., Fujii, S. & Matsui, I. Crystal structure of a core domain of stomatin from Pyrococcus horikoshii Illustrates a novel trimeric and coiled-coil fold. *J Mol Biol* **376**, 868-878 (2008). https://doi.org:10.1016/j.jmb.2007.12.024
33 Brand, J. *et al.* A stomatin dimer modulates the activity of acid-sensing ion channels. *EMBO J* **31**, 3635-3646 (2012). https://doi.org:10.1038/emboj.2012.203
34 Takekawa, N. *et al.* Structure of Vibrio FliL, a New Stomatin-like Protein That Assists the Bacterial Flagellar Motor Function. *mBio* **10** (2019). https://doi.org:10.1128/mBio.00292-19
35 Langhorst, M. F. *et al.* Preformed reggie/flotillin caps: stable priming platforms for macrodomain assembly in T cells. *FASEB J* **20**, 711-713 (2006). https://doi.org:10.1096/fj.05-4760fje
36 Wei, D. *et al.* RAB31 marks and controls an ESCRT-independent exosome pathway. *Cell Res* **31**, 157-177 (2021). https://doi.org:10.1038/s41422-020-00409-1
37 Lu, P. *et al.* Three-dimensional structure of human gamma-secretase. *Nature* **512**, 166-170 (2014). https://doi.org:10.1038/nature13567
38 Alexandrov, A. *et al.* A facile method for high-throughput co-expression of protein pairs. *Mol Cell Proteomics* **3**, 934-938 (2004). https://doi.org:10.1074/mcp.T400008-MCP200
39 Scheich, C., Kummel, D., Soumailakakis, D., Heinemann, U. & Bussow, K. Vectors for co-expression of an unrestricted number of proteins. *Nucleic Acids Res* **35**, e43 (2007). https://doi.org:10.1093/nar/gkm067
40 Schneider, C. A., Rasband, W. S. & Eliceiri, K. W. NIH Image to ImageJ: 25 years of image analysis. *Nat Methods* **9**, 671-675 (2012). https://doi.org:10.1038/nmeth.2089
41 Zheng, S. Q. *et al.* MotionCor2: anisotropic correction of beam-induced motion for improved cryo-electron microscopy. *Nat Methods* **14**, 331-332 (2017). https://doi.org:10.1038/nmeth.4193
42 Zhang, K. Gctf: Real-time CTF determination and correction. *J Struct Biol* **193**, 1-12 (2016). https://doi.org:10.1016/j.jsb.2015.11.003
43 Kimanius, D., Dong, L., Sharov, G., Nakane, T. & Scheres, S. H. W. New tools for automated cryo-EM single-particle analysis in RELION-4.0. *Biochem J* **478**, 4169-4185 (2021). https://doi.org:10.1042/BCJ20210708
44 Emsley, P., Lohkamp, B., Scott, W. G. & Cowtan, K. Features and development of Coot. *Acta Crystallogr D Biol Crystallogr* **66**, 486-501 (2010). https://doi.org:10.1107/S0907444910007493
45 Jumper, J. *et al.* Highly accurate protein structure prediction with AlphaFold. *Nature* **596**, 583-589 (2021). https://doi.org:10.1038/s41586-021-03819-2
46 Varadi, M. *et al.* AlphaFold Protein Structure Database: massively expanding the structural coverage of protein-sequence space with high-accuracy models. *Nucleic Acids Res* **50**, D439-D444 (2022). https://doi.org:10.1093/nar/gkab1061
47 Afonine, P. V. *et al.* Real-space refinement in PHENIX for cryo-EM and crystallography. *Acta Crystallogr D Struct Biol* **74**, 531-544 (2018). https://doi.org:10.1107/S2059798318006551

48 Chen, V. B. *et al.* MolProbity: all-atom structure validation for macromolecular crystallography. *Acta Crystallogr D Biol Crystallogr* **66**, 12-21 (2010). https://doi.org:10.1107/S0907444909042073

49 Pettersen, E. F. *et al.* UCSF Chimera--a visualization system for exploratory research and analysis. *J Comput Chem* **25**, 1605-1612 (2004). https://doi.org:10.1002/jcc.20084

50 Guo, Q. *et al.* In Situ Structure of Neuronal C9orf72 Poly-GA Aggregates Reveals Proteasome Recruitment. *Cell* **172**, 696-705 e612 (2018). https://doi.org:10.1016/j.cell.2017.12.030

51 Hagen, W. J. H., Wan, W. & Briggs, J. A. G. Implementation of a cryo-electron tomography tilt-scheme optimized for high resolution subtomogram averaging. *J Struct Biol* **197**, 191-198 (2017). https://doi.org:10.1016/j.jsb.2016.06.007

52 Khavnekar, S., Erdmann, P. & Wan, W. TOMOMAN: Streamlining Cryo-electron Tomography and Subtomogram Averaging Workflows Using TOMOgram MANager. *Microscopy and microanalysis : the official journal of Microscopy Society of America, Microbeam Analysis Society, Microscopical Society of Canada* **29**, 1020 (2023). https://doi.org:10.1093/micmic/ozad067.516

53 Kremer, J. R., Mastronarde, D. N. & McIntosh, J. R. Computer visualization of three-dimensional image data using IMOD. *Journal of structural biology* **116**, 71-76 (1996). https://doi.org:10.1006/jsbi.1996.0013

54 Tegunov, D. & Cramer, P. Real-time cryo-electron microscopy data preprocessing with Warp. *Nature methods* **16**, 1146-1152 (2019). https://doi.org:10.1038/s41592-019-0580-y

55 Lamm, L. *et al.* MemBrain v2: an end-to-end tool for the analysis of membranes in cryo-electron tomography. *bioRxiv*, 2024.2001.2005.574336 (2024). https://doi.org:10.1101/2024.01.05.574336

56 Nickell, S. *et al.* TOM software toolbox: acquisition and analysis for electron tomography. *Journal of structural biology* **149**, 227-234 (2005). https://doi.org:10.1016/j.jsb.2004.10.006

57 Chaillet, M. L. *et al.* Extensive Angular Sampling Enables the Sensitive Localization of Macromolecules in Electron Tomograms. **24**, 13375 (2023).

58 Bharat, T. A. & Scheres, S. H. Resolving macromolecular structures from electron cryo-tomography data using subtomogram averaging in RELION. *Nature protocols* **11**, 2054-2065 (2016). https://doi.org:10.1038/nprot.2016.124

Figures

Fig. 1

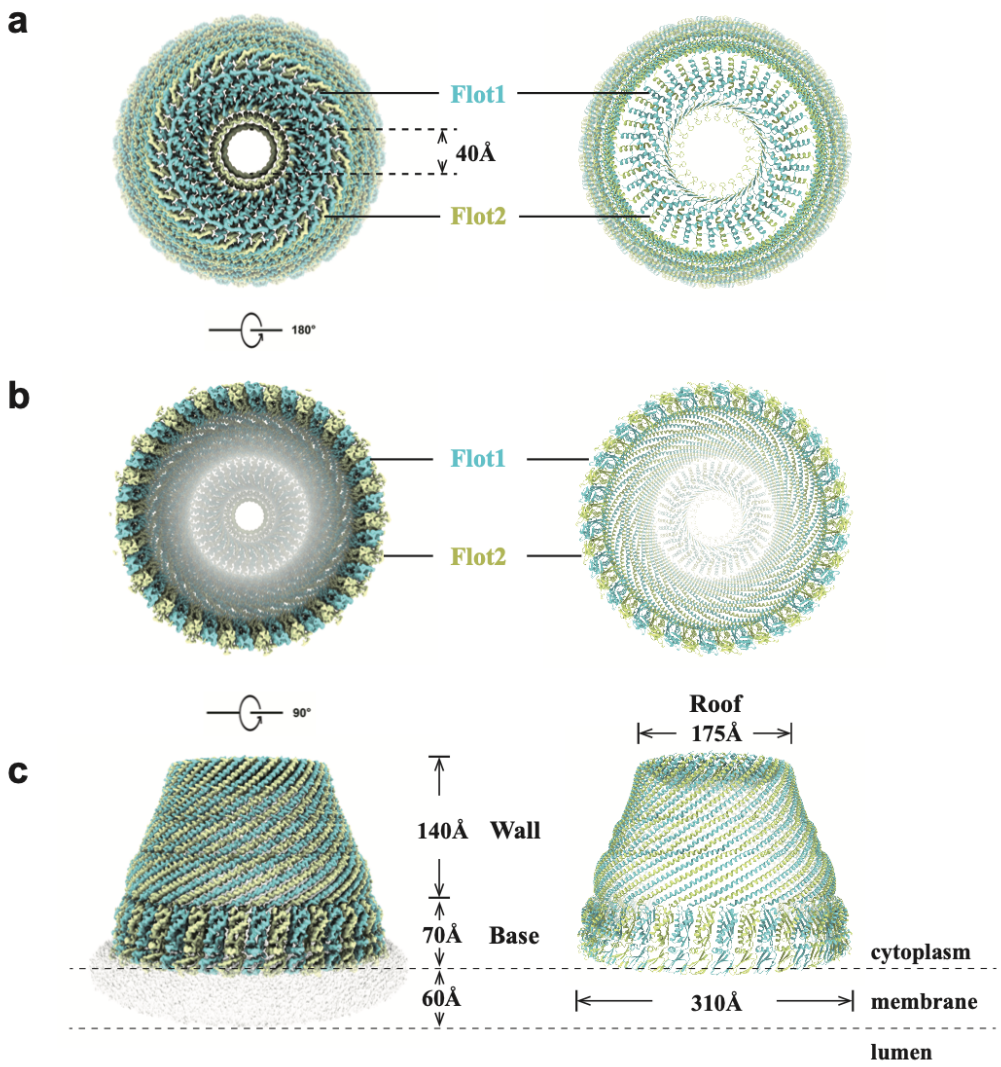

Fig. 1. The overall structure of the FLOT1/FLOT2 complex.

a–c, Ninety-degree rotated views of the cryo-EM density map and atomic model of the FLOT1/FLOT2 complex with 22-fold symmetry. The complex is a dome-shaped structure composed of tightly coiled α-helices as the single-layer wall.

a, Top view (cytoplasmic view) of the cryo-EM map (left) and atomic model (right) of the FLOT1/FLOT2 complex.

b, Bottom view (periplasmic view) of the cryo-EM map (left) and atomic model (right) of the FLOT1/FLOT2 complex.

c, Side view of the cryo-EM map (left) and atomic model (right) of the FLOT1/FLOT2 complex. Subunits of FLOT1 and FLOT2 are colored cyan and yellow, respectively.

Fig. 2

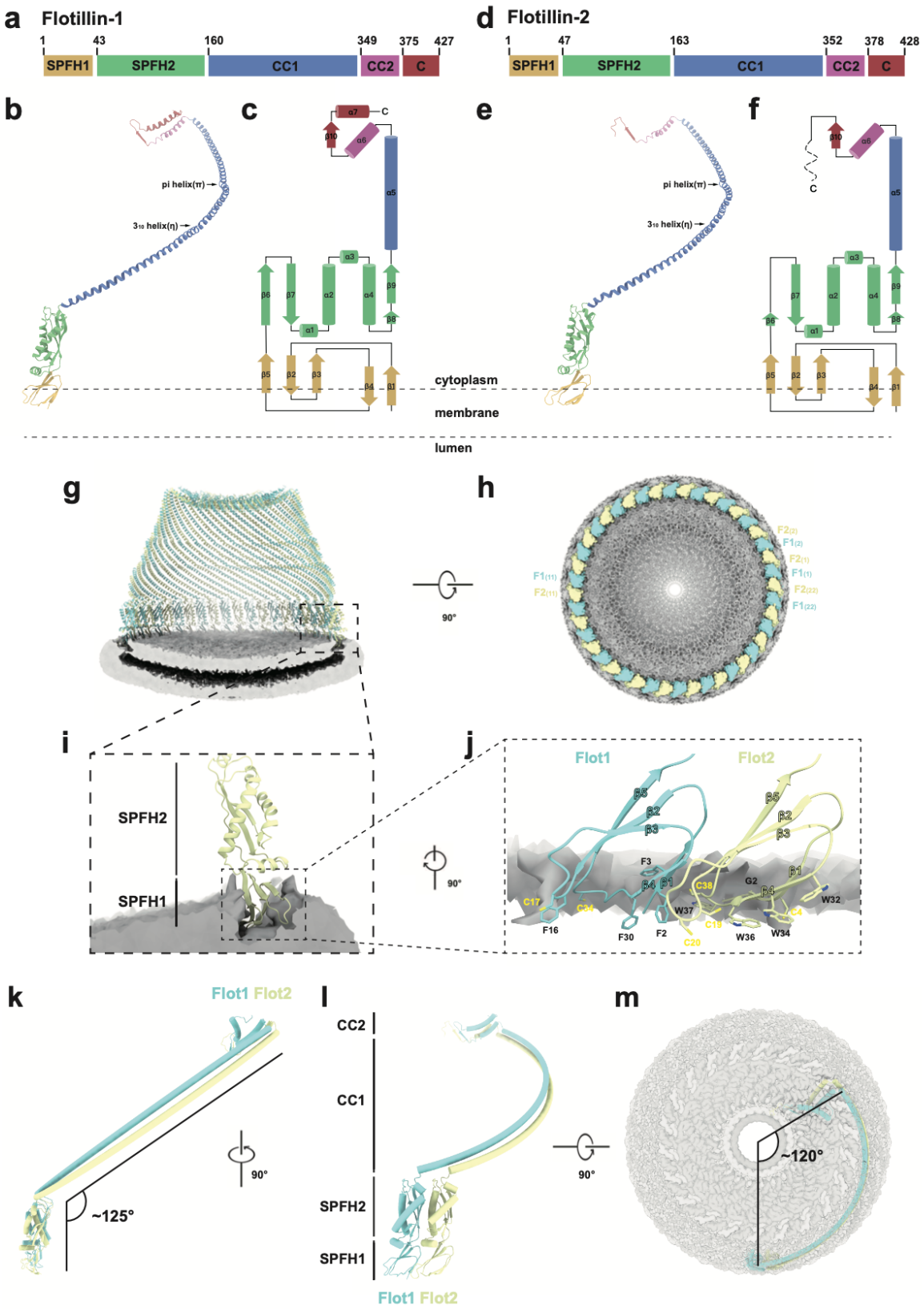
a
Flotillin-1
1
43
160
349
375
427
SPFH1
SPFH2
CC1
CC2
C
d
Flotillin-2
1
47
163
352
378
428
SPFH1
SPFH2
CC1
CC2
C
b
c
e
f
pi helix(π)
3₁₀ helix(η)
cytoplasm
membrane
lumen
g
h
90°
i
j
SPFH2
SPFH1
Flot1
Flot2
90°
k
Flot1 Flot2
~125°
90°
l
m
CC2
CC1
SPFH2
SPFH1
90°
~120°
Flot1 Flot2

Fig. 2. Structures and the membrane association of FLOT1 and FLOT2.

a, d, Schematic illustration of the conserved domain organization of FLOT1 and FLOT2, with individual domains separately colored. SPFH1, gold; SPFH2, green; coiled coil 1(CC1), blue; CC2, purple; C- terminal domain (CTD), red.

b, c, The atomic model (**b**) and the secondary structure topology of FLOT1 (**c**). Secondary structural motifs are colored as in **a**.

e, f, The atomic model (**e**) and the secondary structure topology of FLOT2 (**f**). Secondary structural motifs are colored as in **d**.

g–j, SPFH1 domains of FLOT1 and FLOT2 are peripheral membrane domains inserted in the inner leaflet of the membrane. Subunits of FLOT1 and FLOT2 are colored cyan and yellow, respectively. Detergent density is colored gray.

g, Vertical cross-section view of the atomic model of the FLOT1/FLOT2 complex with the low-pass filtered cryo-EM density map of detergent micelle superimposed, in the position of the axis of symmetry.

h, Horizontal cross-section view of the low-pass filtered cryo-EM density map of the FLOT1/FLOT2 complex with detergent micelle, in the position of the SPFH1 region. 22 FLOT1 and 22 FLOT2 subunits interlacedly arranged as a circle. Protomers of FLOT1 and FLOT2 are numbered anti-clockwisely.

i, Zoomed-in view of the SPFH regions of the FLOT1/FLOT2 complex.

j, Zoomed-in view of the SPFH1 regions of the FLOT1/FLOT2 complex with ninety-degree rotation, with the removal of detergent density in the foreground. Aromatic residues (F2, F3, F16 and F30 of FLOT1; W32, W34, W36 and W37 of FLOT2) are inserted in the membrane. Cystine residues (C34 of FLOT1; C4, C19 and C20 of FLOT2), which are reported to be palmitoylated, and glycine residue (G2 of FLOT2), which is reported to be myristoylated, are all buried in membrane. The covalent attachment of these fatty acids contribute to the membrane association of the FLOT1/FLOT2 complex.

k–m, Side views (**k, l**) and top view (**m**) of one unit cell of the FLOT1/FLOT2 complex (one FLOT1 and one FLOT2 subunit). Subunits of FLOT1 and FLOT2 are colored cyan and yellow, respectively.

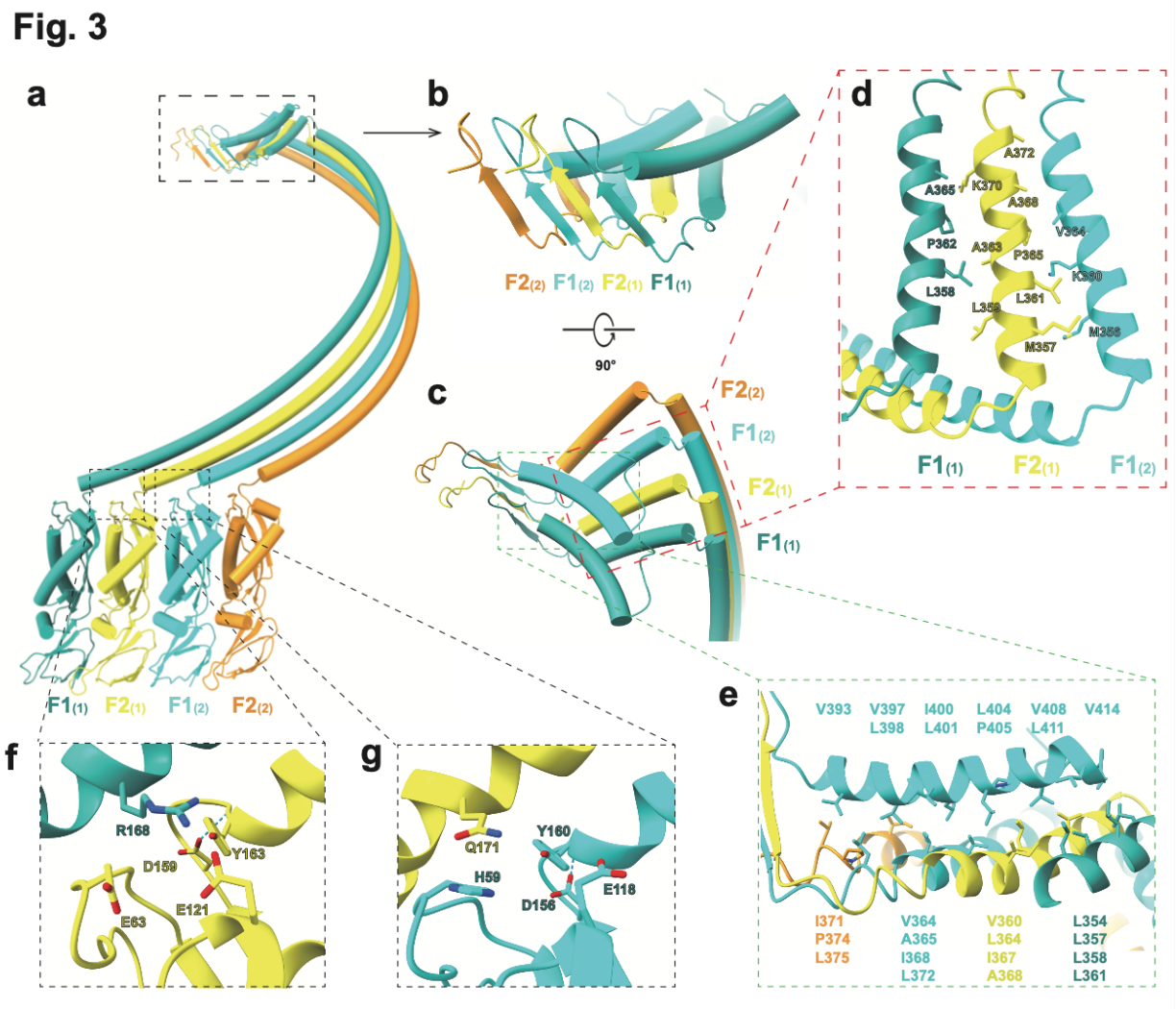

Fig. 3. Key interactions between FLOT1 and FLOT2.

a–g, Side view (**a**) and zoomed-in views (**b–g**) of the four distinctly colored protomers.

b–e, Packing of the four protomers in the cap region of the FLOT1/FLOT2 complex.

d, e, In the cap region, the CC2 region of F2(1) contacts adjacent CC2 regions of F1(1) and F1(2) (**d**); the α-helix in the CTD region of F1(2) contacts four CC2 regions of F1(1), F2(1), F1(2) and F2(2)(**e**). Residues involved in the detailed interactions are labeled. Hydrophobic interactions are dominant in the cap region.

f, g, Detailed interactions among the head end of CC1 regions and SPFH domains (β6-β7 loop and α3 helix) of F1 and F2, including hydrogen bonds between D159 of F2(1) and main-chain atoms of Y163 of F2(1)(**f**), and between D156 of F1(2) and main-chain atoms of Y160 of F1(2)(**g**). E63, E121 and Y163 of F2(1) form a negative potential pocket for R168 of F1(1)(**f**). H59, E118 and Y160 of F1(2) also form a pocket for Q171 of F2(1)(**g**), facilitating multiple polar interactions. These residues are highly conserved between the two flotillin homologs.

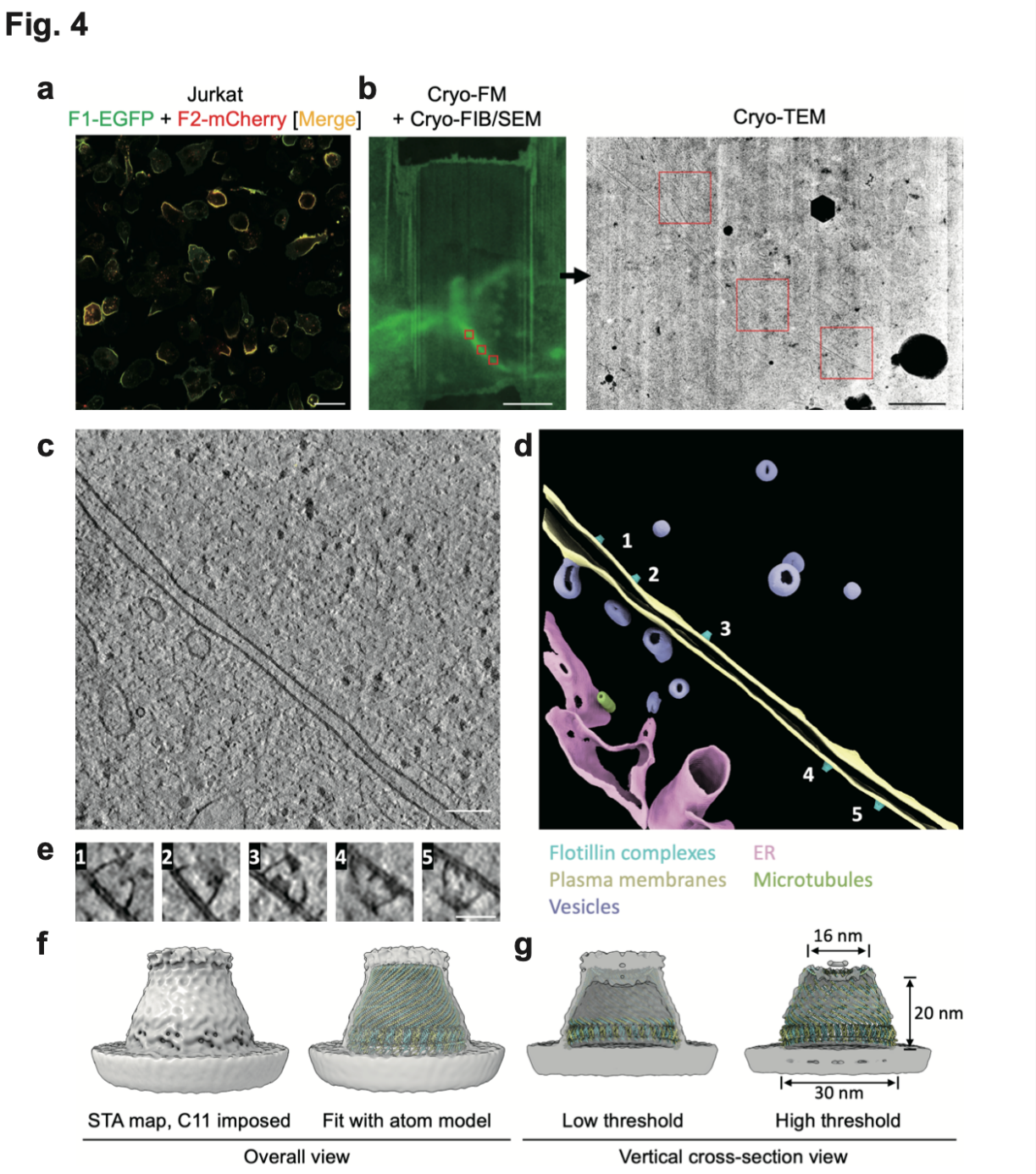

Fig. 4. Visualization of FLOT1/FLOT2 complex in situ.

a, Jurkat cells stably expressing FLOT1-EGFP and FLOT2-mCherry exhibit colocalization at the caps or uropods, as visualized by fluorescence microcopy.

b, Correlative cryo-light and electron microscopy workflow. Regions of interest identified by fluorescence microscopy serve as guide for subsequent tomographic tilt series collection by cryo-EM.

c, A 1.2 nm thick tomographic slice acquired within the area containing the GFP signal (corresponding to flotillin complexes).

d, 3D rendering of the tomogram shown in **c**. Flotillin complexes, plasma membranes, vesicles, ER and microtubules are colored as indicated. Selected flotillin complexes magnified in **e** are indicated by numbers.

e, Tomographic slices zoomed in on the representative flotillin complexes identified within the tomogram shown in panel (c). Notably, the side views of these complexes exhibit variability in shape. Additionally, some complexes (3 and 4, for example) contain internal regions of increased electron density.

f, g, Subtomogram averaging result of flotillin complexes (**f**) and its vertical cross-section views (**g**) at different contour levels. The model of flotillin complexes built with SPA map was fitted in to the STA maps for comparation.

Scale bars, 20 µm (**a**), 5 µm (left panel in **b**), 1 µm (right panel in **b**), 120 nm (**c**) and 30 nm (**e**).

Fig. 5

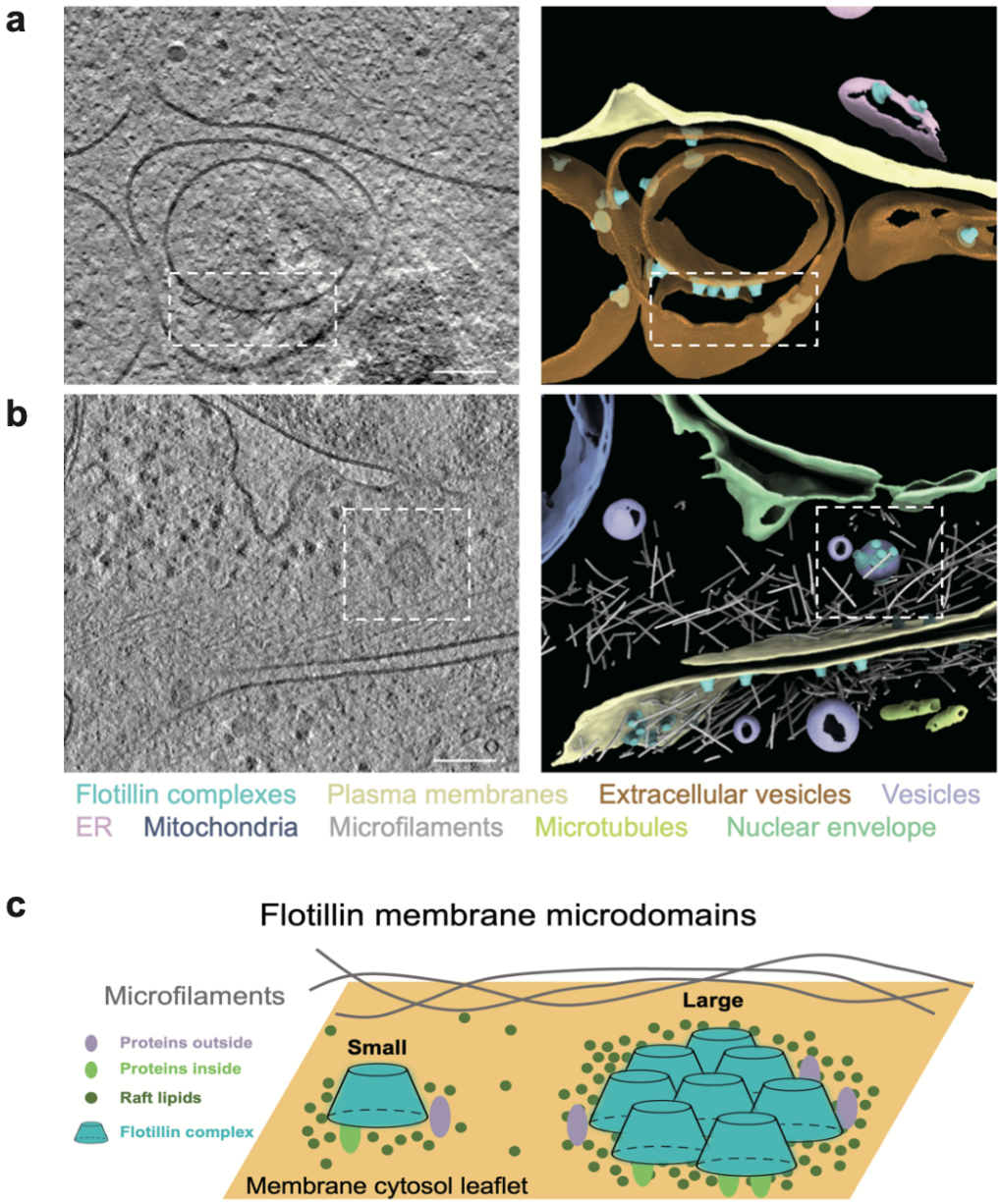

Fig. 5. Organization of FLOT1/FLOT2 complexes in membrane microdomain.

a, b, Tomographic slice (left) and corresponding 3D rendering (right) of representative tomograms acquired from regions identified by flotillin complex fluorescence signal. Subcellular components are colored as indicated.

a, Flotillin complexes are distributed on the cytosol leaflet of plasma membrane and endosomes, as well as the luminal leaflet of extracellular vesicles (specifically, the inner leaflet of the outer membrane and the outer leaflet of the inner vesicles). The boxed region highlights a cluster of flotillin complexes in extracellular vesicles.

b, Flotillin complexes distributed on plasma membrane and endosomes demonstrates their close proximity to actin.

c, Proposed model of flotillin membrane microdomain. An individual flotillin complex along with recruited raft-associated lipids and proteins constitute a specialized minimal membrane microdomain, and can serve as a unit to cluster with others. This clustering, leads to the lateral segregation of regional membranes, ultimately resulting in the formation of large functional membrane microdomains.

Tomographic slices are 1.2 nm thick. Scale bars, 120 nm (**a** and **b**).